PNAS RESEARCH ARTICLE | CELL BIOLOGY

Miat and interacting protein Metadherin maintain a stem-like niche to promote medulloblastoma tumorigenesis and treatment resistance

Kai-Lin Peng[a], Harish N. Vasudevan[a,b], Dennis T. Lockney[a], Rachel Baum[a], Ronald C. Hendrickson[c], David R. Raleigh[b,d,1], and Adam M. Schmitt[a,1]

Edited by Bradley Bernstein, Dana-Farber Cancer Institute, Boston, MA, 02215; received March 4, 2022; accepted August 9, 2022 by Editorial Board Member Jeannie T. Lee

Long noncoding RNAs (lncRNAs) play essential roles in the development and progression of many cancers. However, the contributions of lncRNAs to medulloblastoma (MB) remain poorly understood. Here, we identify *Miat* as an lncRNA enriched in the sonic hedgehog group of MB that is required for maintenance of a treatment-resistant stem-like phenotype in the disease. Loss of *Miat* results in the differentiation of tumor-initiating, stem-like MB cells and enforces the differentiation of tumorigenic stem-like MB cells into a nontumorigenic state. *Miat* expression in stem-like MB cells also facilitates treatment resistance by down-regulating p53 signaling and impairing radiation-induced cell death, which can be reversed by therapeutic inhibition of *Miat* using antisense oligonucleotides. Mechanistically, the RNA binding protein Metadherin (Mtdh), previously linked to resistance to cytotoxic therapy in cancer, binds to *Miat* in stem-like MB cells. Like the loss of *Miat*, the loss of *Mtdh* reduces tumorigenicity and increases sensitivity to radiation-induced death in stem-like MB cells. Moreover, Miat and Mtdh function to regulate the biogenesis of several microRNAs and facilitate tumorigenesis and treatment resistance. Taken together, these data reveal an essential role for the lncRNA *Miat* in sustaining a treatment-resistant pool of tumorigenic stem-like MB cells.

Miat | Metadherin | long noncoding RNA | medulloblastoma

Significance

Here we identify that the long noncoding RNA Miat is induced by oncogenic signaling in medulloblastoma to maintain the self-renewal capacity of tumorigenic stem-like medulloblastoma cells and elicit resistance to cytotoxic therapy. Miat and the interacting RNA binding protein Metadherin contribute to a mechanism that promotes tumorigenesis and treatment resistance and regulates the biogenesis of some microRNAs involved in these processes.

Medulloblastoma (MB) is the most common malignant brain tumor in children (1). Treatment with high-dose chemotherapy and craniospinal irradiation can cure MB, but frequently at the expense of neurocognitive toxicities (2). Tumor classifications based on molecular profiling, dividing the disease into sonic hedgehog (Shh), WNT, group 3, and group 4, have revealed distinct pathogenic drivers of the disease and differentiated prognostic groups. However, attempts to de-intensify therapy in WNT group tumors, which have the best prognoses, resulted in increased risks of treatment failure (3, 4). Therefore, there is a great need to understand the mechanisms of treatment resistance in order to identify novel therapeutic options to enhance the therapeutic window of treatments for MB. Stem-like cancer cells have been postulated to be a reservoir of tumorigenic potential and treatment resistance in MB and other brain tumors (5–8). Identifying and targeting mechanisms that maintain treatment-resistant stem-like MB cells could provide an opportunity to reduce the risk of treatment failure and ultimately support strategies to de-escalate the curative cytotoxic regimen.

The Shh group of MB accounts for ∼30% of patients with the disease. Outcomes in Shh MB are highly variable and include favorable and unfavorable subtypes. Indeed, Shh MBs with *TP53* mutations account for some of the worst prognoses, potentially due to deficiencies in p53-dependent cell death following cytotoxic therapy (9, 10). p53 signaling also plays an important role in preventing cell dedifferentiation, and down-regulation of p53 is a requirement for the generation of induced pluripotent stem cells and stem-like cancer cells (11, 12). Furthermore, subpopulations of stem-like MB cells have been associated with treatment resistance (7, 8, 13). Therefore, understanding the mechanisms that facilitate the maintenance of stem-like MB and their treatment resistance could improve treatment outcomes in the disease.

Long noncoding RNAs (lncRNAs) are increasingly recognized as central actors in cancer phenotypes and function to direct transcription factor or chromatin regulators to specific regions of the genome, regulate RNA processing and stability, or modulate protein–protein interactions that regulate protein function or stability, among many other functions (14). While the functional effects of lncRNAs are diverse, most molecular mechanisms involve lncRNA interactions of one or more classes of cellular macromolecules, DNA, RNA, and/or protein (15). LncRNA-dependent molecular mechanisms are reported to contribute to each of the hallmark phenotypes of cancer, including regulating

Author affiliations: [a]Division of Translational Oncology, Department of Radiation Oncology, Memorial Sloan Kettering Cancer Center, New York, NY, 10065; [b]Department of Radiation Oncology, University of California San Francisco, CA, 94143; [c]Microchemistry and Proteomics, Memorial Sloan Kettering Cancer Center, New York, NY, 10065; and [d]Department of Neurological Surgery, University of California San Francisco, CA, 94143

Author contributions: K.-L.P., D.R.R., and A.M.S. designed research; K.-L.P., H.N.V., D.T.L., R.B., R.C.H., and A.M.S. performed research; K.-L.P., H.N.V., D.R.R., and A.M.S. contributed new reagents/analytic tools; K.-L.P., H.N.V., D.T.L., R.B., R.C.H., D.R.R., and A.M.S. analyzed data; and K.-L.P., D.R.R., and A.M.S. wrote the paper.

The authors declare no competing interest.

This article is a PNAS Direct Submission. B.B. is a guest editor invited by the Editorial Board.

[1]To whom correspondence may be addressed. Email: david.raleigh@ucsf.edu or schmitta@mskcc.org.

This article contains supporting information online at http://www.pnas.org/lookup/suppl/doi:10.1073/pnas.2203738119/-/DCSupplemental.

Published September 6, 2022.

cellular proliferation, tumor suppression, invasion, and metastasis, among many other cancer phenotypes (14). Our prior work has demonstrated that an lncRNA, DINO, promotes p53 protein stability and signaling in response to DNA damage and is recurrently silenced in human cancers as a means of escaping p53-dependent tumor suppression (16, 17). While lncRNAs have received relatively little attention in the mechanisms of MB development, recent work has demonstrated remarkable diversity of lncRNA expression in MB (18). Since many lncRNAs mediate mechanisms that are highly tissue selective or context specific and ~40% of lncRNAs are expressed in the brain, they are attractive targets for drug development because toxicity and off-target effects are anticipated to be minimal, if their mechanisms and physiologic role can be identified (19, 20). Advances in antisense drug development that allow for efficient targeting and degradation of RNAs, including lncRNAs, by systemic or central nervous system (CNS)–restricted drug delivery raise the tantalizing possibility of targeting lncRNAs for therapeutic intervention in CNS cancers (21, 22). This identification of therapeutically targetable lncRNAs involved in the maintenance of MB cells with a stem-like phenotype could augment conventional therapy, improve tumor control, and potentially allow for the de-escalation of cytotoxic therapy to reduce treatment toxicity.

MIAT was initially identified as a myocardial infarction–associated transcript (23) that more recently has been identified to be especially enriched in neural tissues and has been associated with various diseases including schizophrenia and Parkinson's disease (24–26). Mice genetically deficient in *Miat* were found to be fertile and generally healthy with only a mild hyperactivity phenotype (27). MIAT is a nuclear lncRNA that defines a distinct and characteristic subnuclear domain, where it was previously reported to interact with the CELF3 and SF1 proteins to regulate alternative splicing by sequestering these factors away from the splicing machinery (28).

Here, we report that Miat is a highly expressed lncRNA in Shh MB and is dynamically expressed during cerebellar development. *Miat* is regulated by Shh and Myc signaling in MB cells. Miat is essential for the maintenance of a tumorigenic and treatment-resistant stem-like population in MB. We find that Miat interacts with the RNA binding protein Metadherin (Mtdh) in MB cells and that a Mtdh knockout phenocopies the loss of Miat, resulting in impaired maintenance of the tumorigenic stem-like MB cell phenotype and increased sensitivity to radiotherapy. We further find that Miat and Mtdh both regulate the abundance of microRNAs previously associated with tumorigenesis and therapy resistance in cancer models, identifying the regulation of microRNA abundance as a candidate mechanism for the Miat and Mtdh phenotype in MB.

Results

Identification of lncRNAs associated with Shh MB. To define lncRNA candidates that could participate in Shh MB differentiation, we identified lncRNAs that were differentially expressed in Shh MB using RNA sequencing (RNA-seq) of tumors from *Math1-Cre*, SmoM2^{C} mice, which are frequently used to model the disease (29). Here, the expression of a constitutively active, oncogenic point mutation of *Smo* (*SmoM2*^{c}) is restricted to cerebellar granule neuron progenitors (CGNPs) using the conditional transgene *Math1-Cre*. RNA-seq of *Math1-Cre*, *SmoM2*^{c} MB revealed that 605 annotated lncRNAs were differentially expressed (≥ two-fold change; false discovery rate [FDR] ≤ 0.05) in tumors compared to age-matched normal cerebella (Fig. 1*A*) (29). A majority of the differentially expressed lncRNAs were located in intergenic regions (62%) or were antisense to other genes (37%) (Fig. 1*B*). We examined whether lncRNAs differentially expressed in MB were regulated during cerebellar development, since dysregulation of morphogen signaling associated with neurodevelopment is one of the principal drivers of MB development (30–32). Of the 605 lncRNAs differentially expressed in MB, we identified 114 lncRNAs that changed dynamically during CGNP differentiation and cerebellar development, 44 genes that had increased expression in MB revealed high expression early in normal cerebellar development followed by down-regulation at later states (Fig. 1*C*, red line), and 70 genes with low expression in MB compared to normally developing cerebellum were generally up-regulated later in cerebellar development compared to early developmental stages (Fig. 1*C*, green line). To further enrich for lncRNAs that contribute to Shh MB, we filtered lncRNAs differentially expressed in the Shh group of human MB compared to other groups. Using expression data from previously published human MB datasets (33, 34), we identified 10 MB-associated lncRNAs that changed dynamically during cerebellum differentiation and for which expression differed in the Shh group of MB compared to other groups (Fig. 1*D*). Among these lncRNAs, *MIAT* was of particular interest since *MIAT* expression was the highest in human Shh MB compared to other groups of MB in two different cohorts (Fig. 1*E*) and was expressed most highly in the Shh-β subgroup of high-risk infant Shh MB (Fig. 1*F*) (18, 35). Since *Miat* was highly expressed in the cerebellum of *Math1-Cre*; *SmoM2*^{c} mice with MB at postnatal day 35, compared to normal cerebella from *SmoM2*^{c} mice at the same age (Fig. 1*G*), we examined the dynamics of *Miat* during earlier stages of cerebellar development and MB formation. In early postnatal mice, *Miat* was highly expressed at the earliest stages of cerebellar development coinciding with periods of CGNP neurogenesis but was repressed at later stages of normal cerebellar development following CGN differentiation (Fig. 1*H*, black line). In contrast, *Miat* expression in postnatal *Math1-Cre*, SmoM2^{C} mice that were developing MB increased over time during MB formation (Fig. 1*H*, red line). Taken together, these results indicate that *MIAT* is a developmentally regulated lncRNA enriched specifically in human Shh MB and animal models of the disease.

Miat is induced by oncogenic signaling pathways to sustain a stem-like state. We next aimed to identify how *Miat* is regulated to understand its elevated expression in Shh group MB compared to other groups of MB. To study the role of *Miat* in Shh MB, we isolated MB cells from *Math1-Cre*, *SmoM2*^{c} MB by in vitro propagation in defined, serum-free neural stem cell medium, which was previously shown to facilitate in vitro propagation of tumorigenic mouse MB cells that grow in a Shh-dependent manner (36–39). We confirmed the ability of these cells to form MB tumors following engraftment in the posterior fossa of mice, demonstrating they are tumorigenic Shh MB cells and can serve as a model system for oncogenic Shh signaling in MB (*SI Appendix*, Fig. 1*A*). In these MB cells, treatment with smoothened agonist (SAG) induced the expression of *Miat* while the Shh antagonist cyclopamine down-regulated *Miat* expression, indicating that the Shh signaling regulates the expression of *Miat* (Fig. 2*A*). To understand how *Miat* is regulated in response to Shh signaling, we performed knockdown of Gli2, n-myc, and myc, transcriptions that drive oncogenic signaling in MB, and examined the effect on *Miat* expression. Knockdown of Gli2 modestly decreased the expression of *Miat*, while knockdown of n-myc or c-myc substantially down-regulated *Miat* expression (Fig. 2*B* and *SI Appendix*, Fig. 2*A*). In

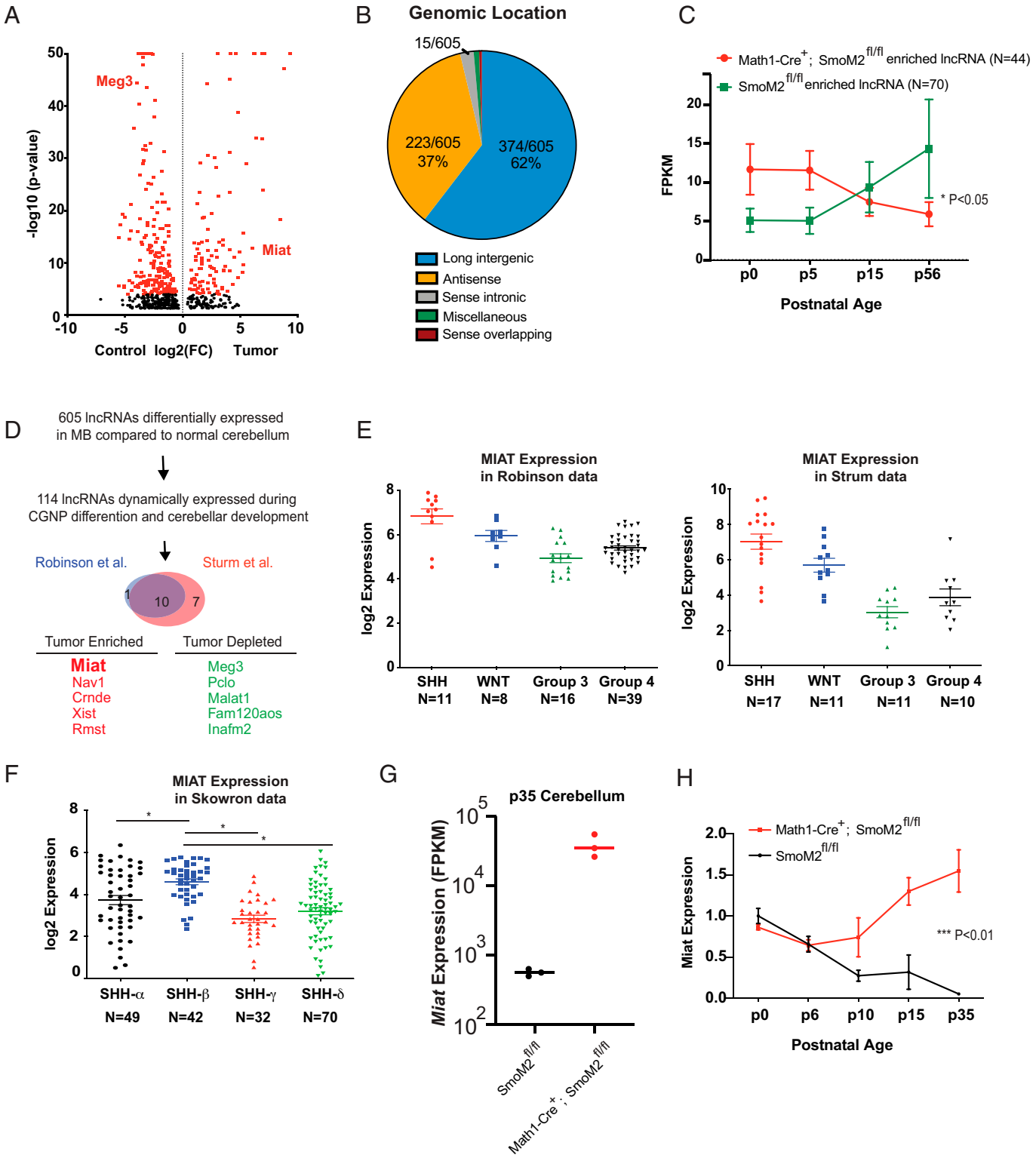

Fig. 1. *Miat* is a developmentally regulated lncRNA associated with Shh MB. (*A*) Volcano plot generated by RNA sequencing of the MBs from Math1-Cre^{+}, SmoM2$^{fl/fl}$ mice relative to the normal cerebella of P35 SmoM2$^{fl/fl}$ littermate controls. There are 605 genes differentially expressed with an FDR <0.05 and differentially expressed lncRNAs in both tumor and control groups, applying a P value < 0.0001 as the threshold (red dots). LncRNAs of particular interest are identified. FC, fold change. (*B*) Relative genomic localization of differentially expressed lncRNAs. (*C*) Differentially expressed lncRNAs during normal mouse cerebellum development. Cerebellum RNA-seq data analyzed from Pal et al. (30). FPKM of genes enriched in MB cerebella from Math1-cre+, SmoM2$^{fl/fl}$ mice (red line, n = 44) in comparison to normal cerebella from cre-, SmoM2$^{fl/fl}$ mice (green line, n = 70). (*D*) Flowchart illustrating criteria to identify candidate lncRNAs involved in Shh MB development. (*E*) *MIAT* expression in human MB patients from Robinson et al. (33) (*Left*) and Sturm et al. (34) (*Right*) datasets. (*F*) *MIAT* expression in human SHH type of MB from Skowron et al. dataset (18). (*G*) FPKM values for Miat from RNA-seq of P35 normal cerebellum from SmoM2$^{fl/fl}$ and MB containing cerebella from Math1-cre+, SmoM2$^{fl/fl}$ mice at P35, from reference (29). (*H*) *Miat* expression in the cerebella of Math1-cre+, SmoM2$^{fl/fl}$ mice (red line) during medulloblastoma formation and during normal cerebellum development in cre-, SmoM2$^{fl/fl}$ mice (black line) from postnatal day 0 through 35, fragments per kilobase of transcript per million mapped reads (FPKM). Miat expression was quantified by qRT-PCR using total RNA extracted from cerebella at each time point. All data were normalized to the value of Miat in SmoM2 fl/fl (wild-type) cerebella at p0. p0, n = 5; p6, n = 6; p10, n = 5; p15, n = 5; p35, n = 4.

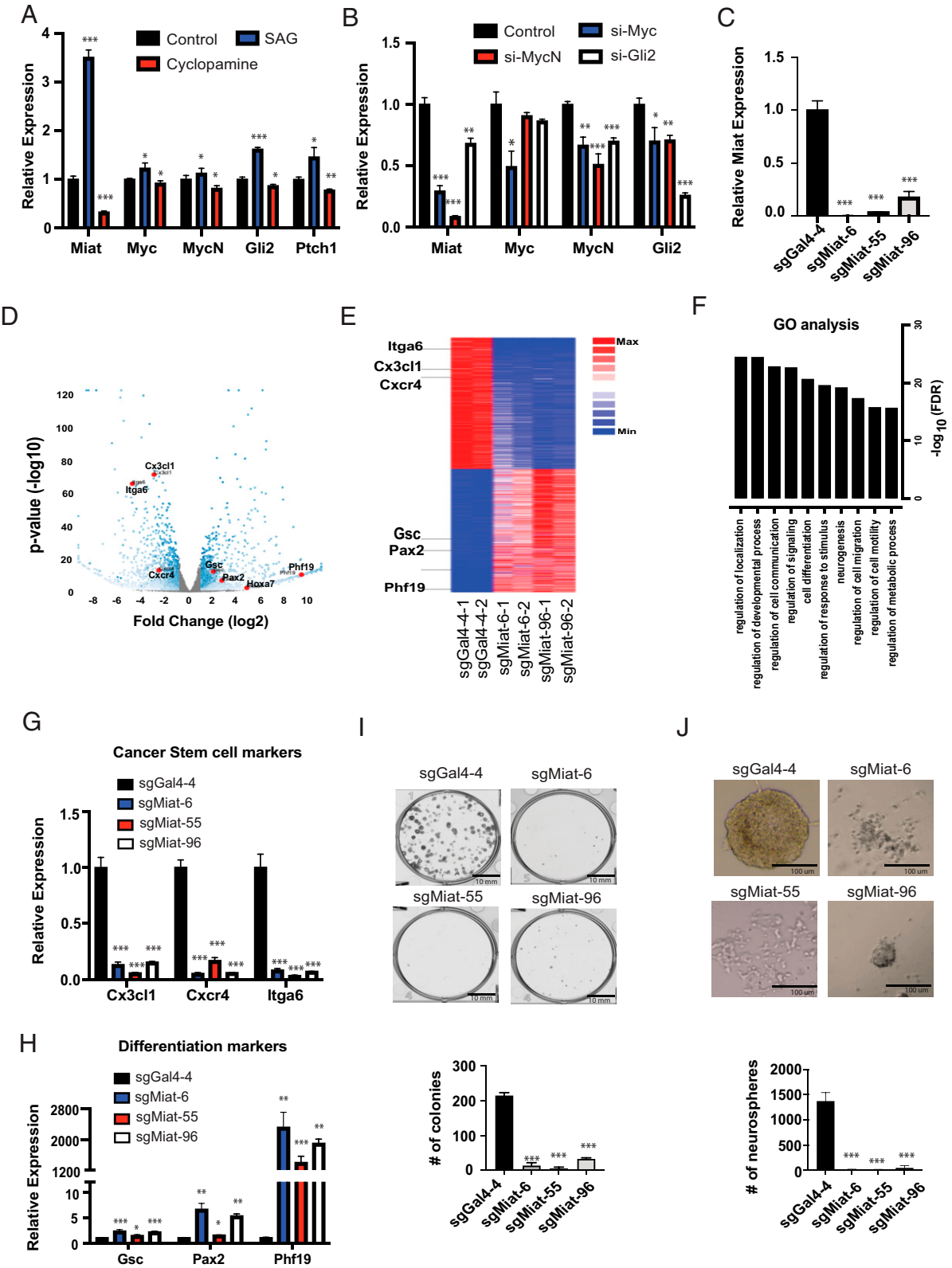

Fig. 2. *Miat* is induced by oncogenic Shh signaling to maintain a stem-like niche of MB cells. (*A*) Gene expression as measured by qRT-PCR of indicated Shh pathway genes in stem-like MB cells treated with SAG, Shh agonist, cyclopamine, Shh signaling antagonist, or vehicle only as a control ($n = 3$). (*B*) Expression of selected genes in stem-like MB cells after knockdown of transcription factors Gli2, n-Myc, and c-Myc, as measured by qRT-PCR ($n = 3$). (*C*) qRT-PCR of *Miat* expression in stem-like MB cells with three sgRNAs targeting Cas9 to *Miat* or control nontargeting sgRNA (Gal4-4). (*D* and *E*) Differentially expressed genes as measured by RNA-seq from 2 sgGal4-4, 2 sgMiat-6, and 2 sgMiat-96 MB cells. There are 3,386 genes differentially expressed with an FDR <0.05 and differentially expressed genes in both experimental (sgMiat) and control (sgGal4-4) groups, applying a P value < 0.0001 as threshold (red dots); genes of particular interest are identified in volcano plot (*D*) and heatmap (*E*). (*F*) Gene ontology (GO) terms associated with differentially expressed genes in *Miat* promoter knockout stem-like MB cells compared to controls. (*G* and *H*) Expression of genes associated with cancer stem cells (*G*) or stem cell differentiation (*H*) in stem-like MB cells with indicated sgRNAs targeting *Miat* for Cas9 or nontargeting control (Gal4-4) ($n = 3$). (*I* and *J*) Promoter knockout of *Miat* impaired the ability to form colonies and neurospheres. Colony formation (*I*) and neurosphere formation (*J*) in stem-like MB cells with indicated sgRNAs targeting *Miat* with Cas9 or nontargeting control. *Bottom*: quantitation data of triplicate experiments.

human DAOY cells, a human Shh MB cell line, anti-MYC chromatin immunoprecipitation (ChIP) recovered a region of the *MIAT* promoter that is also associated with the histone H3K27ac defined enhancer element upstream of *MIAT* that is specific to Shh group MB (40), indicating that the Shh group–specific enhancer is an myc-bound enhancer (*SI Appendix*, Figs. 1*B* and 2*B*). These data demonstrate that *Miat* is an lncRNA regulated by the Shh pathway and myc family transcription factors in MB.

Mouse Miat is an 8,760 nt lncRNA with seven exons located on chromosome 5 without clearly delineated functional domains (*SI Appendix*, Fig. 2*C*). To elucidate the function of *Miat,* we endeavored to generate MB stable cells with *Miat* knockdown or knockout of the full-length transcript using CRISPR systems. Our initial attempts to down-regulate *Miat* with dCas9-KRAB (CRISPRi) could not achieve efficient gene knockdown (*SI Appendix*, Fig. 2 *C* and *D*). We previously observed that a small insertion into the promoter of the lncRNA *Dino* efficiently inhibited *Dino* transcription by ablating the promoter (16). We thus generated stable cell lines each expressing one of three unique small guide RNAs (sgRNAs) that targeted the promoter region of *Miat* near the transcription start site (three different sgRNAs, each used to construct a different stable cell line). Expression of these sgRNAs in combination with Cas9, but not a nontargeting control sgRNA, generated indels in the promoter of *Miat*, and qRT-PCR revealed that this strategy resulted in highly efficient reduction of *Miat* expression by each of the three independent sgRNAs, consistent with a promoter knockout effect (Fig. 2*C*). RNA-seq revealed that *Miat* promoter knockouts resulted in substantial changes in genes, both mRNAs and lncRNAs, associated with neurogenesis, development, motility, and cellular metabolism Gene Ontology (GO) terms (Fig. 2 *D*–*F*). While both mRNA and lncRNA expression was altered by *Miat* promoter knockouts, biases in mRNA and lncRNA quantification due to the use of polyA selection procedures to generate RNA-seq libraries precluded an analysis of the relative functional impact of Miat on lncRNAs in comparison to mRNAs from these data. qRT-PCR validated that promoter knockouts of *Miat* reduced the expression of pluripotent cancer stem cell markers such as *Cx3cl1*, *Cxcr4*, and *Itga6* (Fig. 2*G*) and up-regulated markers of differentiation, like *Gsc*, *Pax2*, and *Phf19* (Fig. 2*H*) in all 3 *Miat* promoter knockout stable cell lines. Since these data suggest that the loss of *Miat* reduced markers of stemness and increased markers of differentiation, we examined the ability of these MB cells to differentiate in response to retinoic acid. Indeed, treatment with retinoic acid down-regulated genes associated with a stem-like phenotype, including Sox2 and Nanog, indicating that Miat is regulating the differentiation of cells with a neural stem cell–like phenotype (*SI Appendix*, Fig. 2*E*). Since *Miat* promoter knockouts in stem-like MB cells were associated with increased expression of differentiation markers and reduced expression of genes associated with the stem-like phenotype, we examined the effect of *Miat* promoter knockouts on in vitro colony formation and neurosphere formation, assays of a stem-like cancer cell phenotype. *Miat* promoter knockouts almost completely impaired the ability of stem-like MB cells to form colonies (Fig. 2*I*) and neurospheres (Fig. 2*J*) but had only a minimal effect on in vitro cell proliferation (*SI Appendix*, Fig. 2*F*). In contrast, *Miat* knockdown using CasRx had no effect on colony formation in Med1–MB cells, a differentiated mouse MB cell line derived from a *Ptch1*$^{+/-}$ mouse (*SI Appendix*, Fig. 2 *G* and *H*) (41, 42). Therefore, *Miat* is induced by canonical oncogenic signaling pathways in MB to maintain a stem-like niche of MB cells.

Miat down-regulates p53-dependent gene expression and facilitates treatment resistance. Our RNA-seq data also demonstrated that all three promoter knockouts of *Miat* notably modulated canonical p53-dependent genes (FDR adjusted $P < 10^{-4}$ by Kyoto Encylopedia of Genes and Genomes pathway analysis). qRT-PCR confirmed that promoter knockouts of *Miat* were associated with increased expression of p53-regulated genes involved in apoptosis and cell cycle arrest, including *Puma*, *Bax*, and *Cdkn1a*, which are necessary for the efficient killing of MB cells by cytotoxic therapies such as radiation (Fig. 3*A*) (43). This finding raised the possibility that *Miat* expressing stem-like MB cells may be relatively resistant to cell death by cytotoxic therapies since p53 signaling is a major determinant of therapeutic efficacy and treatment outcomes in MB (9, 10). As stem-like cancer cells and impaired p53-dependent cell death have been linked to resistance to cytotoxic therapies, we were interested to examine the implications of p53 dysregulation by *Miat* on MB responses to radiation therapy, a backbone of the curative treatment for MB. Consistent with a role for *Miat* in resistance to cytotoxic therapy, promoter knockouts of *Miat* in stem-like MB cells significantly increased the fraction of dead stem-like MB cells following radiation therapy and lowered the threshold for cytotoxicity in stem-like MB cells following radiation therapy (Fig. 3 *B* and *C* and *SI Appendix*, Fig. 3*A*). In contrast, knockdown of *Miat* in Med1 cells, a differentiated mouse Shh MB cell line that expresses *Miat*, had no effect on sensitivity to radiation, suggesting that *Miat*'s role in promoting treatment resistance is limited to the stem-like MB cells (*SI Appendix*, Fig. 3*B*). Nuclear lncRNAs can be efficiently targeted for therapeutic inhibition and, since *Miat*$^{-/-}$ mice are fertile and have no apparent developmental or health problems, *Miat* is an attractive therapeutic target with a potentially low risk of toxic side effects (27). To examine whether *Miat* can be therapeutically targeted, we generated custom Antisense Locked Nucleic Acid (LNA) GapmeRs to knockdown *Miat* in stem-like MB cells. Two GapmeRs achieved efficient knockdown in stem-like MB cells and induced the p53-dependent genes *Puma*, *Bax*, and *Cdkn1a*, similar to promoter knockouts of *Miat* (Fig. 3 *D* and *E*). A single treatment of stem-like MB cells with *Miat* GapmeRs increased cell death at baseline and following radiation therapy and reduced colony formation in vitro (Fig. 3 *F* and *G*). Thus, *Miat* down-regulates the expression of p53 pathway effector genes in stem-like MB cells and maintains a treatment-resistant stem-like MB cell phenotype, making Miat a potential therapeutic target to sensitize treatment-resistant stem-like MB cells.

Mtdh binds Miat to regulate miRNA biogenesis involved in MB. LncRNA mechanisms are frequently mediated by their interactions with other cellular macromolecules such as protein, RNA, or DNA. To identify the mechanisms by which *Miat* functions to maintain the stem-like MB phenotype, we next characterized the proteins that colocalized with *Miat* in stem-like MB cells. Single-guide RNAs (sgRNAs) targeting *Miat* guided the APEX2-dCas13 fusion protein to *Miat*-enriched nuclear domains, and proteins were subsequently labeled by proximity biotinylation (44). Mass spectrometry of recovered biotinylated proteins identified Mtdh, also known as LYRIC, as a highly enriched protein in samples isolated from stem-like MB cells expressing APEX2-dCas13 and sgRNAs targeting *Miat* (*SI Appendix*, Fig. 4*A* and Table S1). Mtdh is an RNA binding protein previously shown to contribute to mechanisms of chemoresistance and is required for the tumor-initiating capacity of cancer cells (45–47). RNA immunoprecipitation with anti-Mtdh specifically retrieved *Miat* in stem-like MB cells, confirming that Mtdh and *Miat* interact

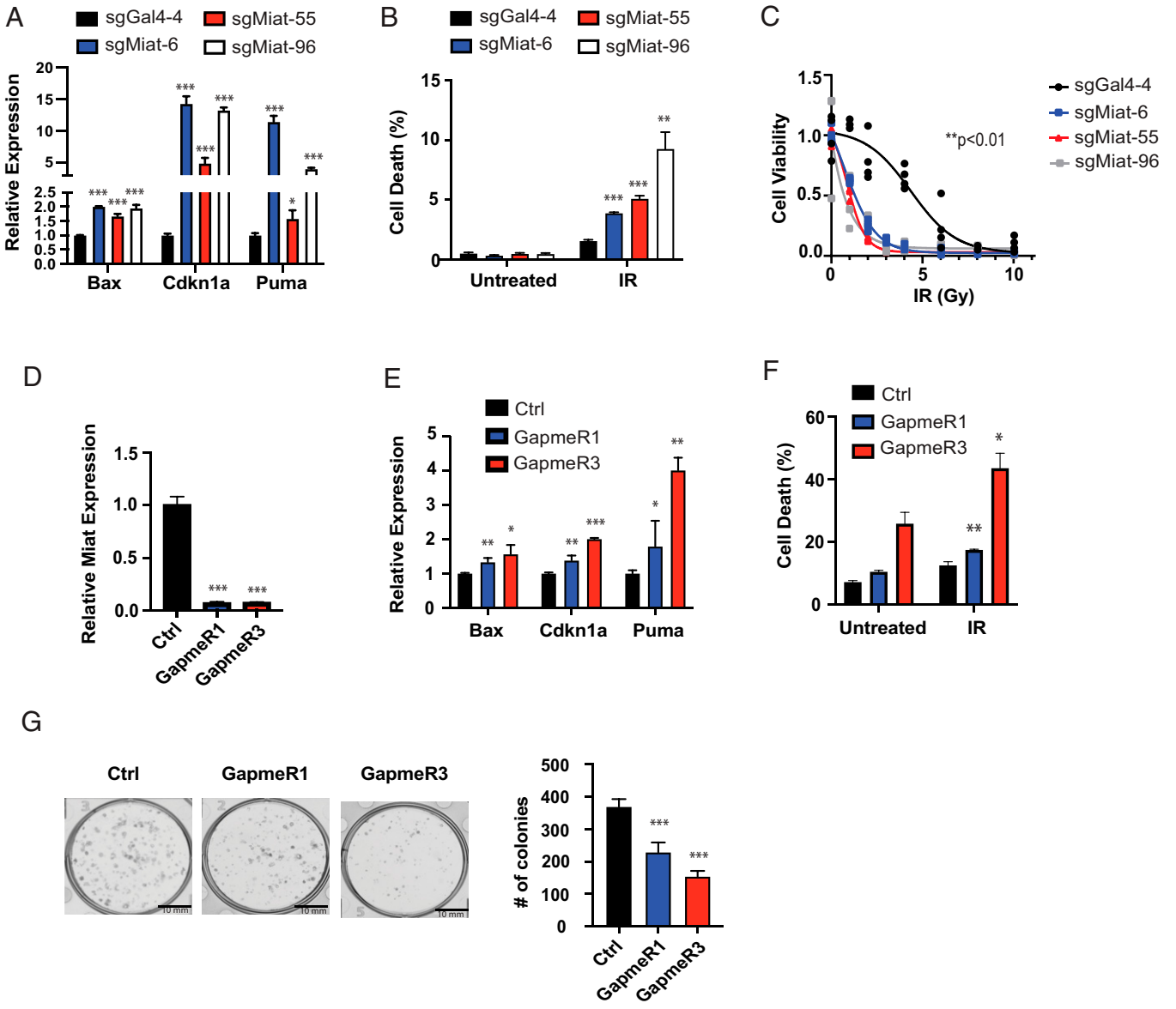

Fig. 3. *Miat* sustains a treatment-resistant stem-like MB niche. (*A*) Expression of p53-dependent genes *Bax*, *Cdkn1a*, and *Puma* in stem-like MB cells with sgRNAs targeting Cas9 to *Miat* or control nontargeting sgRNA (Gal4-4) ($n = 3$). (*B*) Fraction of dead cells as measured by propidium iodide (PI) staining 24 h after irradiation (IR; 5 Gy) in stem-like MB cells with sgRNAs targeting Cas9 to *Miat* or control nontargeting sgRNA (Gal4-4) ($n = 3$). (*C*) Cell viability as measured by 3-(4,5-dimethylthiazol-2-yl)-5-(3-carboxymethoxyphenyl)-2-(4-sulfophenyl)-2H-tetrazolium (MTS) assay 48 h after increasing doses of IR (0, 1, 2, 3, 4, 6, 8, 10 Gy) in stem-like MB cells with sgRNAs targeting Cas9 to *Miat* or control nontargeting sgRNA (Gal4-4) ($n = 4$). (*D* and *E*), Expression of *Miat* (*D*) and p53-dependent genes *Bax*, *Cdkn1a*, and *Puma* (*E*) in stem-like MB cells treated with GapmeRs targeting *Miat* or control ($n = 3$). (*F*) Fraction of dead cells as measured by PI staining 24 h after IR (5 Gy) in stem-like MB cells treated with GapmeRs targeting *Miat* or control ($n = 3$). (*G*) Colony formation in stem-like MB cells treated with GapmeRs targeting *Miat* or control; *Right*: quantification of colony formation ($n = 3$). ***P value < 0.001; **P value < 0.01, *P value < 0.05 by Student t test.

in cells (Fig. 4*A*). Transient knockdown of Mtdh using small interfering RNAs (siRNAs) or Cas9 knockout of *Mtdh* ($Mtdh^{-/-}$) in stem-like MB cells impaired neurosphere formation in vitro, similar to promoter knockouts of *Miat* (Figs. 4 *B* and *C* and *SI Appendix*, Fig. 4 *B* and *C*). Furthermore, gene expression in $Mtdh^{-/-}$ stem-like MB cells suggested changes associated with differentiation, similar to *Miat* promoter knockouts in stem-like MB cells, with down-regulation of the stem cell marker *Cxcr4* and up-regulation of the differentiation marker *Pax2* (Fig. 4 *D* and *E*)). $Mtdh^{-/-}$ stem-like MB cells, similarly, had increased expression of the p53 effector genes *Puma*, *Bax*, and *Cdkn1a* and reduced stem-like MB cell viability following radiation therapy (Fig. 4*F* and *SI Appendix*, Fig. 4 *D* and *E*). Since $Mtdh^{-/-}$ mice manifest a deficit in small RNA biogenesis (48), we performed small RNA-seq in *Miat* promoter knockouts and $Mtdh^{-/-}$ stem-like MB cells, revealing that the loss of either *Miat* and *Mtdh* resulted in substantial changes in the abundance of several small RNAs (Fig. 4*G* and FDR ≤ 0.05). There was a statistically significant similarity in the effect of *Miat* promoter knockout and *Mtdh* loss on the effect of these small RNAs ($P < 10^{-6}$ by Fisher exact test; Fig. 4*H* and *SI Appendix*, Fig. 4*F*). qRT-PCR confirmed a similar effect for all three *Miat* promoter knockout stable cell lines and two $Mtdh^{-/-}$ lines on several of these microRNAs, including miR-181a-1, which has been associated with cancer initiation; miR-30d, which is amplified in some MB samples and associated with tumorigenesis; and miR-92b, which has been associated with Shh MB and may promote stem cell and cancer proliferation and resistance to cancer treatment (Fig. 4*I*) (49–57). Thus, Mtdh binds to *Miat* to regulate the biogenesis of microRNAs involved in cancer initiation and treatment sensitivity and is necessary for the maintenance of a treatment-resistant stem-like population of MB cells.

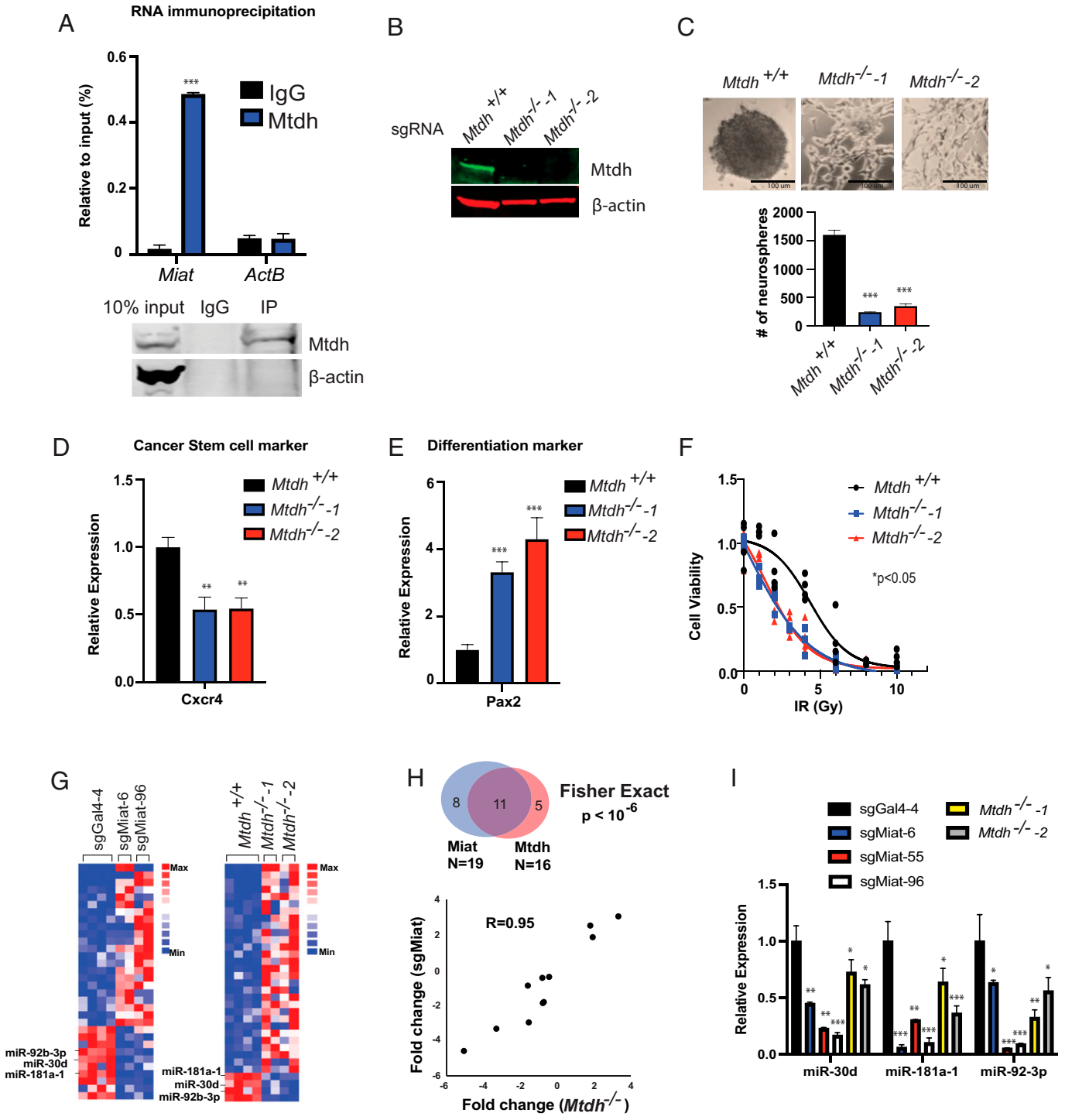

Fig. 4. Miat binds Mtdh to regulate microRNAs involved in stem cell maintenance, tumorigenesis, and treatment resistance. (*A*) RNA immunoprecipitation confirmed the association of Mtdh and *Miat* in stem-like MB cells. (*B*) Western blot of Mtdh and β-actin in stem-like MB cells in two cell $Mtdh^{-/-}$ cell lines generated by CRISPR and $Mtdh^{+/+}$ control. (*C*) Neurosphere formation in $Mtdh^{-/-}$ stem-like MB cells and $Mtdh^{+/+}$ controls ($n = 3$). (*D* and *E*) Expression of genes associated with cancer stem cells (*D*) or stem cell differentiation (*E*) in $Mtdh^{-/-}$ stem-like MB cells and $Mtdh^{+/+}$ controls ($n = 3$). (*F*) Cell viability as measured by MTS assay 48 h after increasing doses of IR (0, 1, 2, 3, 4, 6, 8, 10 Gy in $Mtdh^{+/+}$ and $Mtdh^{-/-}$ stem-like MB cells; $n = 4$ in each group). (*G*) Heat map of differentially expressed small RNAs from small RNA-seq in stem-like MB cells generated with Cas9 and indicated sgRNAs targeting either *Miat* or nontargeting control Gal4-4 (*Left*) and $Mtdh^{+/+}$ and $Mtdh^{-/-}$ stem-like MB cells (*Right*). (*H*) Correlation of magnitude and direction of change in 11 small RNAs that were significantly altered in sgMiat and $Mtdh^{-/-}$ stem-like MB cells compared to controls. *Top*, Venn diagram indicating the overlap in small RNAs altered by sgMiat or Mtdh loss; $P < 10^{-6}$ by the Fisher exact test. (*I*) Expression of miRNAs in stem-like MB cells with indicated sgRNAs targeting either *Miat* with Cas9 or nontargeting control (Gal4-4) and $Mtdh^{-/-}$ stem-like MB cells. ***P value < 0.001; **P value < 0.01; *P value < 0.05 via Student t test.

Miat and Mtdh are essential for tumorigenesis of stem-like MB cells. We next set out to examine whether *Miat* contributes to Shh MB development. We crossed *Math1-Cre*, *SmoM2*^{c} with $Miat^{-/-}$ mice (27) in both $p53^{+/+}$ and $p53^{-/-}$ backgrounds since p53 mutations are strongly associated with the aggressive Shh MB subtype with an exceptionally poor prognosis (58). Homozygous genetic loss of *Miat* prolonged median survival in both $p53^{+/+}$ and $p53^{-/-}$ MB animals, indicating that *Miat* supports MB development in multiple contexts of Shh MB (Fig. 5*A*). Homozygous genetic deletion of *Miat* also

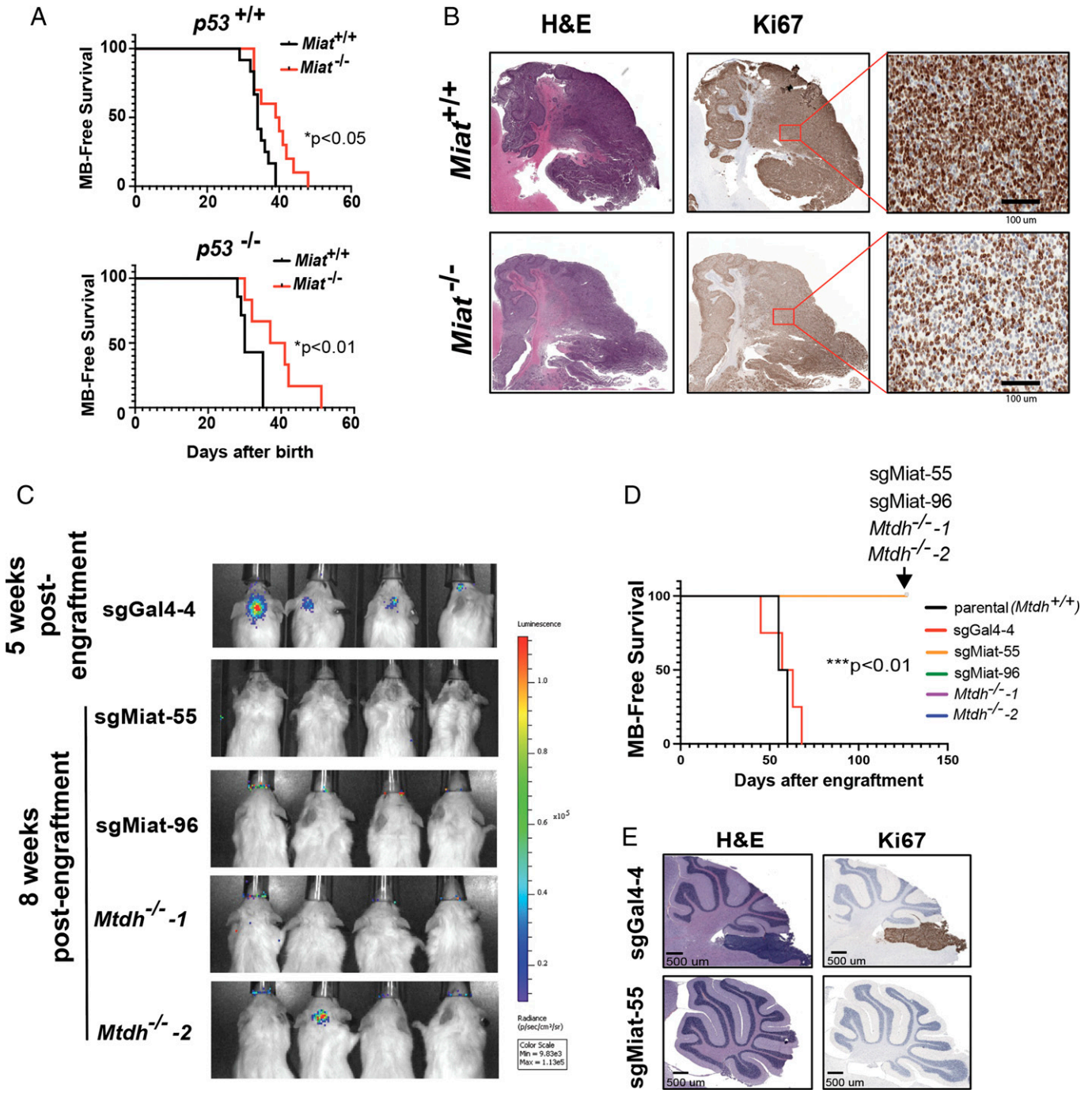

Fig. 5. Miat and Mtdh facilitate MB tumorigenesis. (*A*) *Top*, Kaplan–Meier survival curves in Math1-cre+, SmoM2$^{fl/fl}$ Shh MB mice in the *p53*$^{+/+}$ background; $n = 12$ *Miat*$^{+/+}$ with median survival of 34 d; and $n = 10$ *Miat*$^{-/-}$ with median survival of 39.5 d; *: $P < 0.05$, log-rank test. *Bottom*, Kaplan–Meier survival curves in Math1-cre+, SmoM2^{C} Shh MB mice in the *p53*$^{-/-}$ background; $n = 7$ *Miat*$^{+/+}$ with median survival of 30 d; and $n = 6$ *Miat*$^{-/-}$ mice with a median survival of 38.5 d; **$P < 0.01$, log-rank test. (*B*) Representative H&E and Ki67 stains of midline sagittal sections through the cerebella of Math1-Cre, SmoM2$^{fl/fl}$ *Miat*$^{+/+}$ and *Miat*$^{-/-}$ mice ($n = 3$). (*C*) Orthotopic tumor formation of stem-like MB cells with indicated sgRNAs targeting either *Miat* with Cas9 or nontargeting control (sgGal4-4) or *Mtdh*$^{-/-}$ stem-like MB cells, with luciferase imaging at indicated times after tumor engraftment. Control cell lines generated luminescent tumors detectable by 4 wk after engraftment but *Miat* promoter knockout and *Mtdh*$^{-/-}$ cells had no luminescence at a time point after all control animals had succumbed to MB tumors. (*D*) Kaplan-Meier survival curves for mice orthotopically engrafted with stem-like MB cells with indicated sgRNAs targeting either *Miat* with Cas9 or nontargeting control and in *Mtdh*$^{-/-}$ and *Mtdh*$^{+/+}$ stem-like MB cells. ($n = 4$ in each group). (*E*) Representative H&E and Ki67 stains of midline sagittal sections through the cerebella from either sgGal4-4 or sgMiat-55 mice at the experimental endpoint.

reduced the proliferative fraction of cells as measured by Ki67 staining and partially restored cerebellar architecture (Fig. 5*B*), indicating that *Miat* supports the growth of Shh MB.

While genetically defined mouse models confirmed that *Miat* contributes to the growth of MB, we reasoned that *Miat* and Mtdh may contribute more potently to MB tumor initiation from stem-like cells since the cellular phenotype of *Miat* and Mtdh is pronounced in stem-like MB cells but is not apparent in Med1 cells, a differentiated Shh MB cell line. Parental stem-like MB cells and cells expressing a nontargeting sgRNA readily formed luciferase-expressing MB tumors after engraftment in the posterior fossa and subsequently developed rapidly progressive neurologic symptoms including severe ataxia within 8 wk of engraftment (Fig. 5 *C–E*). However, mice engrafted

with *Miat* promoter knockout stem-like MB cells or *Mtdh*$^{-/-}$ stem-like MB cells have shown no evidence of MB formation by luciferase at 8 wk and had no sign of pathologic evidence of tumor formation (Fig. 5 *C–E*). Hematoxylin and eosin (H&E) and Ki67 staining demonstrated that control stem-like MB cells formed tumors in posterior fossa that were uniformly positive for Ki67; however, no tumor cells were found in mice engrafted with stem-like MB cells with *Miat* promoter knockout (Fig. 5*E*). In sum, these data suggest a model whereby *Miat* and Mtdh are essential for the maintenance of a population of tumorigenic and treatment-resistant stem-like MB cells through the regulation of the biogenesis of a subset of microRNAs (Fig. 5*F*).

Discussion

Despite extensive identification of novel transcripts in the noncoding genome, functional annotation is lacking for the vast majority of these genes and rigorous genetic evidence for lncRNA mechanisms in cancer phenotypes remains rare. However, the association of lncRNAs with neurodevelopmental phenotypes and cellular differentiation suggests that these molecules could mediate critical mechanisms in cancer pathophysiology. The results described here demonstrate that the lncRNA Miat, which is mostly dispensable for normal development and health, nevertheless contributes to critical phenotypes in MB tumorigenesis and treatment resistance. That this contrasts starkly with the need for Miat in normal development and a dispensable role in the tumorigenic potential of differentiated MB cells highlights that lncRNA mechanisms are often exquisitely tissue and context specific. This is further suggested by our observations of some distinctions in the phenotype of stem-like MB cells with acute knockdown of Miat by GapmeRs compared with stem-like MB cells with the stable loss of Miat due to promoter knockouts. Here, acute Miat depletion in stem-like MB cells using GapmeRs, while efficiently knocking down *Miat*, resulted in a less-potent reduction of p53-dependent gene expression and more moderate irradiation-induced cell death compared to stable Miat promoter knockout cells. This finding may indicate that the effects of Miat depletion on cell death result from a combination of dysregulation of p53-dependent gene expression and additional functional effects of chronic Miat depletion on the sensitivity of MB cells to DNA damage–induced cell death.

While our data show that Miat and Mtdh interact in MB cells, the manner by which these two molecules interact and the importance of this interaction to their mechanism in MB cells require future investigation. Our data identified that Mtdh was retrieved by APEX–mass spectrometry targeting Miat and the Mtdh–RNA immunoprecipitation recovered Miat, but these approaches are unable to resolve the precise molecular interaction of Miat and Mtdh. While Mtdh is a known RNA binding protein and a direct interaction with Miat is plausible, an indirect interaction between Mtdh and Miat resulting from subnuclear colocalization or through the formation of a larger macromolecular complex are also possibilities. While promoter knockout of *Miat* and loss of *Mtdh* both elicited a significant effect in the radiation sensitization of MB cells and the activation of p53-dependent gene expression, promoter knockouts of Miat notably produced a more pronounced effect than *Mtdh* knockout in both cases. This finding also suggests that additional factors likely contribute to mechanisms by which Miat functions in MB cells to regulated radiation sensitivity and p53-depedent gene regulation, beyond Mtdh. An alternative explanation is that the loss of Mtdh in MB cells could be partially compensated by other proteins involved in the *Miat* mechanism. Our data demonstrate that Mtdh loss and Miat promoter knockouts result in similar effects on a subset of small RNAs, supporting a conclusion that Miat and Mtdh function in a common mechanism but are insufficient to definitively conclude that the regulation of small-RNA biogenesis is the ultimate mechanism responsible for the observed phenotypes in stem-like MB cells. As previously observed, Miat contributes to the regulation of alternative splicing, in which Mtdh has also been implicated under certain contexts. The shared contribution of Miat and Mtdh to the regulation of microRNAs and alternative splicing suggests that Miat, interacting with a complement of RNA processing factors, may regulate multiple aspects of nuclear processing of both long and short RNA species. Future studies are needed to dissect the contributions of Miat and Miat-associated proteins in the regulation of nuclear RNA processing and how each of these components relates to the multiple crucial phenotypes that Miat regulates in stem-like MB cells.

Finally, these results have identified a therapeutically targetable mechanism that maintains a niche of tumorigenic and treatment-resistant stem-like MB cells that requires the lncRNA *Miat* and its interaction with the protein Mtdh. Extensive prior work in preclinical models indicated that Mtdh-dependent processes would be attractive targets for improving cancer sensitivity to cytotoxic therapy (45, 46), but translation to the clinic has been hampered by the fact that Mtdh has no ligand-binding domain and is considered an undruggable target (59). Further, sterility in *Mtdh*$^{-/-}$ males also limits enthusiasm for drug development target Mtdh due to concerns for toxicity. *Miat* is critical for maintaining the treatment-resistant and tumorigenic potential of stem-like MB cells while being simultaneously dispensable for health and normal development, making it an especially attractive therapeutic target in MB. More broadly, these data suggest that conserved cancer mechanisms thought to be undruggable may be vulnerable to modulation by targeting lncRNAs in the pathway.

Materials and Methods

Mice. C57BL/6 (number 000664), *SmoM2-eYFP*$^{loxP/loxP}$ (number 005130), *Math1-Cre* (number 011104), luciferase (number 005125), and NOD-scid (number 005557) mice were purchased from the Jackson Laboratory. *Miat* (*Gomafu*) null Neo (accession number CDB1377K) mice were acquired from RIKEN (number RBRC10157) (27). p53 null mice were kindly provided by Scott Lowe. Mouse genotyping was performed using Cre, SmoM2, Luc, p53, and Miat primers as indicated. All mice were of the species *Mus musculus* and maintained on a C57BL/6 background over at least five generations and were handled in compliance with all relevant ethical regulations for animal testing and research as specified by the MSK Institutional Animal Care and Use Committee in approved protocol 15–07-011.

Cell culture. Stem-like MB stem cells were cultured according to established protocols (2). Briefly, tumor-bearing cerebellum was retrieved from MB mice. After dissociation using 50% Accutase (Sigma-Aldrich number A6964-100ML), cells were cultured in 0.1% gelatin-coated plates with neurobasal medium (Thermo-Fisher Scientific number 21103049), Pen-Strep, glutamine, N2 (Thermo-Fisher Scientific number 17502048), B27 (-RA) (Thermo-Fisher Scientific number 12587010), hEGF 25 ng/mL (Thermo-Fisher Scientific #PHG0311), and bFGF 25 ng/mL (Thermo-Fisher Scientific number PHG0311). Med1-MB cells were kindly provided by David R. Raleigh and cultured in DMEM with Pen-Strep, glutamine. For clonogenic cell survival assays, 1,000 MB cells or 500 Med1-MB cells were plated per well in triplicate in a 6-well dish and cultured for 9 d. Colonies were fixed with methanol, stained with crystal violet, and counted using GelCount (Oxford Optronix). Edu incorporation was assayed using the Click-iT Plus EdU Alexa Fluor 488 Flow Cytometry Assay Kit (Thermo number C10632). Cell viability was measured using an MTS assay (Promega number G3580) and

propidium iodide (Thermo-Fisher Scientific number P1304MP) either 24 or 48 h after irradiation treatment.

sgRNA design, plasmid construction, lentivirus, retrovirus production, and stable cell line construction. sgRNAs targeting within 200 bp of the annotated TSS of Miat were designed according to Feng Zhang's website (https://zlab.bio/guide-design-resources). Cas9 sgRNAs were cloned into lenti-CRISPRv2 (Addgene number 52961) using the BsmBI site. sgRNA seq: sgGal4-4, AACGACTAGTTAGGCGTGTA; sg*Miat*-6, AGTAGCCCCTTTGTGAGGCG; sg*Miat*-55, CGTTGCTATGGCAGCGCCGC; sg*Miat*-96, GATCGCGCCTCCGACCGTC. sg*Mtdh*-1, CGCCATTGTTCCGCCGGGGG; sg*Mtdh-2*, AGGCGGCCGCTAAGCGGCGT. An APEX2-dCas13 plasmid was purchased from Addgene (number 154939). A pregRNA cloning backbone (Addgene number 109054) was used for APEX-2-dCas13 and CasRx knockdown constructs cloned into the pBabe-zeo vector (Addgene number 1766) with the cutting site NheI. sgRNA cassettes containing three independent sgRNAs were then cloned into the pBabe-zeo-pregRNA vector using golden gate cloning with the restriction site of BbsI. sgRNA sequences of each of the sgRNA arrays are as follows:

Nontargeting control array: CACCGGACGGAGGCTAAGCGTC, CACCGGACGGAGGCTAAGCGTC, CACCGGACGGAGGCTAAGCGTC
sgMiat array A: CAGGACTCAAGCAAAGAGATGT, CACTGAACAGAACTGTATGGTG, TGGTGAAATGTGGAAGATTGGC
sgMiat array B: CCATAAGTGGAGGAATGGTAAG, GACAGATAATATCTCATCCTTC, CTGTGTAAAAGATCTGCCTTAG

Lentiviral vectors and retroviral vectors were transfected into LentiX 293T cells (Takara number 632180) and Phoenix-293T, respectively, and supernatants were concentrated using a Lenti-X or Retro-X concentrator prior to use. Three days after infection of MB cells with sgRNAs and Cas9 or Cas13 expression constructs were infected, cells were selected with antibiotics for 3 d and then underwent three to four passages to expand the cell population before freezing multiple aliquots for long-term storage in liquid nitrogen. All gene expression and cellular experiments were performed with cells within three passages after recovery from cryostorage. In vivo tumorigenesis experiments used cells less than six passages after recovery, due to the need for a larger number of cells for the experiment. In all experiments, sustained efficacy of reduced *Miat* expression in *Miat* promoter knockout cell lines was confirmed by qRT-PCR at the time the experiment was performed, after cells were recovered from cryopreservation.

Antisense oligo, siRNA, and compound administration. Stem-like MB cells were nucleofected with either 250 nM antisense oligos (ASOs) or 100 nM siRNAs using the Mouse Neuron Nucleofector Kit (Lonza number VVPG-1001) according to the manufacturer's instructions. Next, 48 h after nucleofection, cells were harvested for qRT-PCR or Western blot. Sequencing of ASO negative control is as follows: +A*+A*+C*A*C*G*T*C*T*A*T*A*+C*+G*+C; *Miat* GapmeR1, +T*+A*+G*C*A*C*T*T*T*G*A*T*T*+G*+A*+C; *Miat* GapmeR3, +A*+G*+A*T*G*C*A*G*G*C*G*A*T*+T*+A*+G (+, locked nucleic acids; *, phosphorothioated DNA–based). siRNAs were purchased from the Thermo Fisher silencer select (number 4390771) with *Myc* (siRNA number s70225), *MycN* (number s70661), *Gli2* (number s66727), and *Mtdh* (number s84566). For Shh agonist and antagonist treatment, stem-like MB cells were treated with either 250 nM SAG (Sigma-Aldrich number SML1314) or 1 μM cyclopamine (Stemcell number 72072) for 24 h, and then RNA was extracted for expression analysis. For retinoic acid (RA) treatment, MB was treated with 500 nM RA (Sigma-Aldrich number R2625) for 48 h.

Tumor sphere assay. Tumor sphere assay (hanging drop method) was performed as described previously (60). Briefly, 10,000 cells were seeded in the form of 30 μL drops on the inverted lid of the 10 cm Petri dish, while the dish contained Ca^{2+}-and Mg^{2+} -free PBS supplemented with penicillin 100 (U/mL) and streptomycin (100 μg/mL). After 48 hours, pictures were taken of the cells using a microscope.

Mice allograft model and survival analyses. For allograft studies, 1 μL containing 1 million stem-like MB cells was injected into the cerebellum of NOD-scid mice (JAX number 005557) at a position of 0 × 2 × 1.5 mm with respect to lambda by a stereotactic frame. Tumor-bearing mice were monitored daily for health status and movement abnormalities. Tumor luminescence images were acquired by IVIS Spectrum. All mice were euthanized in accordane with the approved IACUC protocol at the onset of symptoms, including 10% weight loss, ataxia, or lethargy. The age of the animal at the time of harvest due to tumor symptoms was recorded. Kaplan–Meier curves were plotted using GraphPad Prism, and significance was calculated using the logrank test. The Kaplan–Meier method was used to estimate survival, and logrank tests were used to compare survival between experimental groups. Cohorts of four mice were each engrafted with stable cell lines from each of the three sgRNAs targeting *Miat*, sgRNA non-targeting control, and the two $Mtdh^{-/-}$ cell lines. The cage housing four mice engrafted with sgMiat-6 was found flooded, and the severely ill mice had to be euthanized in accordane with the approved IACUC protocol. While necropsy demonstrated no evidence of tumor, these data were removed from the analysis since the mice were euthanized in accordane with the approved IACUC protocol at a time earlier than control animals developed any signs of MB formation.

Histology and immunohistochemistry. For histological analysis, mouse brains were removed and fixed with 4% PFA overnight and then transferred to 70% alcohol and embedded in paraffin. Sections were then stained with H&E or with Ki67 antibody, which were done by the core facility laboratory of comparative pathology at Memorial Sloan Kettering Cancer Center.

ChIP. ChIP was performed as described previously (61). Primer sequences are listed in *SI Appendix*, Table S2. Significance was calculated by *t* test, and error bars show SEM.

Reverse transcription reactions and qRT-PCR. Total RNAs from mouse tissues or cells were isolated using TRIzol Reagent or RNeasy Plus column, respectively. For detecting the expression of protein-coding genes and lncRNA *Miat*, RNA samples were directly performed by one-step qRT-PCR (Agilent number 600835). For detecting the expression of miRNAs, 10 ng RNA samples were reverse-transcribed to complementary DNA (cDNA) using the TaqMan MicroRNA Reverse Transcription Kit (Thermo-Fisher Scientific number 4366596) and used stem-loop reverse transcription approaches to detect miRNA expression. Actin and U6 served as internal controls for the expression of protein-coding genes and miRNAs, respectively. Relative expression was evaluated with the $2-\Delta\Delta Ct$ method. For the detection of alternative splicing, RNA samples were reverse-transcribed to cDNA by superscript IV Reverse Transcriptase before PCR. All the primer sequences for qRT-PCR are provided in *SI Appendix*, Table S2.

RNA immunoprecipitation. RNA immunoprecipitations were performed as described previously (62). Briefly, stem-like MB cells were fixed by 1% formaldehyde (Thermo-Fisher Scientific number 28908) for 10 min and quenched with 125 mM glycine before harvesting. Cells then were sequentially lysed by nuclear lysis buffer (1.28 M sucrose, 40 mM Tris·HCl pH 7.5, 20 mM MgCl2, and 4% Triton X-100) and RNA immunoprecipitation (RIP) buffer (150 mM KCl, 25 mM Tris pH 7.4, 5 mM EDTA, 0.5 mM DTT, 0.5% Nonidet P-40, RNase inhibitor, and protease inhibitors). Next, 1 μg IgG (Cell Signaling Technology number 2729S) or anti-Mtdh antibody (Proteintech number 13860–1-AP) were incubated with protein lysate and protein A bead (Thermo-Fisher Scientific number 10001D) at 4 °C overnight. After being washed three times by RIP buffer, the coprecipitated RNAs were eluted, extracted, and detected by qRT-PCR. The primer sequences are provided in *SI Appendix*, Table S2.

Western blotting and antibodies. The commercial Abs are listed as follows: Mtdh (Abcam number ab124789), Myc (Abcam number 39688), *N*-Myc (Santa-Cruz number sc53993), β-actin (Abcam number 6276), β-tubulin (Genetex number GTX101279), H3K27ace (Abcam number 4729), mouse IgG (Sigma-Aldrich number12–371), and rabbit IgG (Cell Signaling Technology number 2729S).

APEX labeling and streptavidin bead enrichment of biotinylated proteins. APEX2 labeling was performed as described previously (44). Briefly, 24 h prior to labeling, stem-like MB cells stably expressing APEX2-dCas13 fusion, transposase, and nontarget gRNA or single-guide Miat were treated with doxycycline (400 ng/mL). Then, biotin-phenol (final concentration 500 μM) was directly added into the culture medium for 30 min at 37 °C. Later, H_2O_2 was added to media at a final concentration of 1 mM to induce biotinylation. After very gently swirling for 1 min, the media was decanted as quickly as possible and the cells were washed three times with PBS containing 100 mM sodium

azide, 100 mM sodium ascorbate, and 50 mM 6-hydroxy-2,5,7,8-tetramethylchroman-2-carboxylic acid. The cell pellets were then lysed with RIPA lysis buffer (50 mM Tris, 150 mM NaCl, 0.1% sodium dodecyl sulfate [SDS], 0.5% sodium deoxycholate, 1% Triton X-100, protease inhibitor) followed by streptavidin bead enrichment. Biotinylated proteins were then eluted by boiling the beads in 50 μL 4× protein-loading buffer supplemented with 20 mM DTT and 2 mM biotin and ran on SDS-polyacrylamide gel electrophoresis (PAGE) gel. SDS-PAGE gel then was stained by silver staining. Differential bands underwent liquid chromatography-tandem mass spectrometry to identify the protein ID, listed in *SI Appendix*, Table S1.

RNA preparation for RNA-seq and small RNA-seq analysis. RNA was harvested from stable MB cell lines modified with Cas9 and sgRNAs targeting the promoter. RNA was isolated from cells no later than six passages after antibiotic selection and purified by the Qiagen RNeasy Plus column. RNA integrity was confirmed using the Agilent Bioanalyzer before RNA-seq library preparation. Both RNA-seq and small RNA-seq were performed on the Illumina NovaSEq. 6000 using the protocols of paired-end 150 and single-end 50 reads, respectively. Reads were aligned to the mouse genome mm10 using the spliced-read aligner HISAT2 v2.0.3 with default parameters. Transcript abundance estimation in transcripts per million (TPM) and differential expression analysis were performed using DESeq2 (63). We identified differentially expressed transcripts with an adjusted P value < 0.1 and further filtered significant genes based on an expression cutoff (TPM > 1) and fold-change threshold ($|\log2FC| > 1$). Differential expression in the small RNA-seq datasets were performed used the small RNA-seq pipeline in Basepair. Sequencing data are deposited at GEO accession number GSE205695 and GSE205691.

Data, Materials, and Software Availability. All sequencing data are available in GEO Datases at accession numbers GSE205691 (64) and GSE205695 (65). Plasmids are available upon request. All other data are presented in the figures and *SI Appendix*.

ACKNOWLEDGMENTS. We thank Azusa Tanaka for helpful discussions and comments on the manuscript. Shinichi Nakagawa kindly provided the *Miat*$^{-/-}$ mice. Scott Lowe kindly provided the *p53*$^{-/-}$ mice. This study was supported by funding from NIH R35GM124909 (to A.M.S.), American Cancer Society RSG-19-158-01-RMC (to A.M.S. and R.C.H.), and the Memorial Sloan Kettering Cancer Center (MSKCC) Cancer Center Core Grant P30 CA008748. All animal experiments and procedures were approved by MSKCC's Institutional Animal Care and Use Committee.

1. Q. T. Ostrom *et al.*, CBTRUS statistical report: Primary brain and central nervous system tumors diagnosed in the United States in 2008-2012. *Neuro-oncol.* **17**, iv1–iv62 (2015).
2. A. W. Walter *et al.*, Survival and neurodevelopmental outcome of young children with medulloblastoma at St Jude Children's Research Hospital. *J. Clin. Oncol.* **17**, 3720–3728 (1999).
3. P. A. Northcott *et al.*, Medulloblastomics: The end of the beginning. *Nat. Rev. Cancer* **12**, 818–834 (2012).
4. J. M. Michalski *et al.*, Children's oncology group phase III trial of reduced-dose and reduced-volume radiotherapy with chemotherapy for newly diagnosed average-risk medulloblastoma. *J. Clin. Oncol.* **39**, 2685–2697 (2021).
5. S. Bao *et al.*, Glioma stem cells promote radioresistance by preferential activation of the DNA damage response. *Nature* **444**, 756–760 (2006).
6. M. Diehn *et al.*, Association of reactive oxygen species levels and radioresistance in cancer stem cells. *Nature* **458**, 780–783 (2009).
7. J. K. Ocasio *et al.*, scRNA-seq in medulloblastoma shows cellular heterogeneity and lineage expansion support resistance to SHH inhibitor therapy. *Nat. Commun.* **10**, 5829 (2019).
8. R. J. Vanner *et al.*, Quiescent sox2(+) cells drive hierarchical growth and relapse in sonic hedgehog subgroup medulloblastoma. *Cancer Cell* **26**, 33–47 (2014).
9. A. J. Crowther *et al.*, Radiation sensitivity in a preclinical mouse model of medulloblastoma relies on the function of the intrinsic apoptotic pathway. *Cancer Res.* **76**, 3211–3223 (2016).
10. D. Hambardzumyan *et al.*, PI3K pathway regulates survival of cancer stem cells residing in the perivascular niche following radiation in medulloblastoma in vivo. *Genes Dev.* **22**, 436–448 (2008).
11. H. Hong *et al.*, Suppression of induced pluripotent stem cell generation by the p53-p21 pathway. *Nature* **460**, 1132–1135 (2009).
12. D. F. Tschaharganeh *et al.*, p53-dependent Nestin regulation links tumor suppression to cellular plasticity in liver cancer. *Cell* **158**, 579–592 (2014).
13. D. M. Treisman *et al.*, Sox2^{+} cells in sonic hedgehog-subtype medulloblastoma resist p53-mediated cell-cycle arrest response and drive therapy-induced recurrence. *Neurooncol. Adv.* **1**, vdz027 (2019).
14. A. M. Schmitt, H. Y. Chang, Long noncoding RNAs in cancer pathways. *Cancer Cell* **29**, 452–463 (2016).
15. A. M. Schmitt, H. Y. Chang, Long noncoding RNAs: At the intersection of cancer and chromatin biology. *Cold Spring Harb. Perspect. Med.* **7**, a026492 (2017).
16. A. M. Schmitt *et al.*, An inducible long noncoding RNA amplifies DNA damage signaling. *Nat. Genet.* **48**, 1370–1376 (2016).
17. C. B. Marney *et al.*, p53-intact cancers escape tumor suppression through loss of long noncoding RNA Dino. *Cell Rep.* **35**, 109329 (2021).
18. P. Skowron *et al.*, The transcriptional landscape of Shh medulloblastoma. *Nat. Commun.* **12**, 1749 (2021).
19. S. J. Liu *et al.*, CRISPRi-based genome-scale identification of functional long noncoding RNA loci in human cells. *Science* **355**, aah7111 (2017).
20. M. K. Iyer *et al.*, The landscape of long noncoding RNAs in the human transcriptome. *Nat. Genet.* **47**, 199–208 (2015).
21. G. Arun *et al.*, Differentiation of mammary tumors and reduction in metastasis upon Malat1 lncRNA loss. *Genes Dev.* **30**, 34–51 (2016).
22. R. S. Finkel *et al.*; ENDEAR Study Group, Nusinersen versus sham control in infantile-onset spinal muscular atrophy. *N. Engl. J. Med.* **377**, 1723–1732 (2017).
23. N. Ishii *et al.*, Identification of a novel non-coding RNA, MIAT, that confers risk of myocardial infarction. *J. Hum. Genet.* **51**, 1087–1099 (2006).
24. N. A. Rapicavoli, E. M. Poth, S. Blackshaw, The long noncoding RNA RNCR2 directs mouse retinal cell specification. *BMC Dev. Biol.* **10**, 49 (2010).
25. S. Q. Rao, H. L. Hu, N. Ye, Y. Shen, Q. Xu, Genetic variants in long non-coding RNA MIAT contribute to risk of paranoid schizophrenia in a Chinese Han population. *Schizophr. Res.* **166**, 125–130 (2015).
26. M. Akbari *et al.*, Expression of BDNF-associated lncRNAs in Parkinson's disease. *Metab. Brain Dis.* **37**, 901–909 (2022).
27. J. Y. Ip *et al.*, Gomafu lncRNA knockout mice exhibit mild hyperactivity with enhanced responsiveness to the psychostimulant methamphetamine. *Sci. Rep.* **6**, 27204 (2016).
28. A. Ishizuka, Y. Hasegawa, K. Ishida, K. Yanaka, S. Nakagawa, Formation of nuclear bodies by the lncRNA Gomafu-associating proteins Celf3 and SF1. *Genes Cells* **19**, 704–721 (2014).
29. D. R. Raleigh *et al.*, Hedgehog signaling drives medulloblastoma growth via CDK6. *J. Clin. Invest.* **128**, 120–124 (2018).
30. S. Pal *et al.*, Alternative transcription exceeds alternative splicing in generating the transcriptome diversity of cerebellar development. *Genome Res.* **21**, 1260–1272 (2011).
31. U. Schüller *et al.*, Acquisition of granule neuron precursor identity is a critical determinant of progenitor cell competence to form Shh-induced medulloblastoma. *Cancer Cell* **14**, 123–134 (2008).
32. Z. J. Yang *et al.*, Medulloblastoma can be initiated by deletion of Patched in lineage-restricted progenitors or stem cells. *Cancer Cell* **14**, 135–145 (2008).
33. G. Robinson *et al.*, Novel mutations target distinct subgroups of medulloblastoma. *Nature* **488**, 43–48 (2012).
34. D. Sturm *et al.*, New brain tumor entities emerge from molecular classification of CNS-PNETs. *Cell* **164**, 1060–1072 (2016).
35. F. M. G. Cavalli *et al.*, Intertumoral heterogeneity within medulloblastoma subgroups. *Cancer Cell* **31**, 737–754.e6 (2017).
36. T. A. Read *et al.*, Identification of CD15 as a marker for tumor-propagating cells in a mouse model of medulloblastoma. *Cancer Cell* **15**, 135–147 (2009).
37. R. J. Ward *et al.*, Multipotent CD15+ cancer stem cells in patched-1-deficient mouse medulloblastoma. *Cancer Res.* **69**, 4682–4690 (2009).
38. J. Kim *et al.*, Itraconazole and arsenic trioxide inhibit hedgehog pathway activation and tumor growth associated with acquired resistance to smoothened antagonists. *Cancer Cell* **23**, 23–34 (2013).
39. X. Huang, T. Ketova, Y. Litingtung, C. Chiang, Isolation, enrichment, and maintenance of medulloblastoma stem cells. *J. Vis. Exp.* (43), 2086 (2010).
40. C. Y. Lin *et al.*, Active medulloblastoma enhancers reveal subgroup-specific cellular origins. *Nature* **530**, 57–62 (2016).
41. L. V. Goodrich, L. Milenković, K. M. Higgins, M. P. Scott, Altered neural cell fates and medulloblastoma in mouse patched mutants. *Science* **277**, 1109–1113 (1997).
42. Y. Tang *et al.*, Epigenetic targeting of hedgehog pathway transcriptional output through BET bromodomain inhibition. *Nat. Med.* **20**, 732–740 (2014).
43. A. J. Crowther *et al.*, Tonic activation of Bax primes neural progenitors for rapid apoptosis through a mechanism preserved in medulloblastoma. *J. Neurosci.* **33**, 18098–18108 (2013).
44. S. Han *et al.*, RNA-protein interaction mapping via MS2- or Cas13-based APEX targeting. *Proc. Natl. Acad. Sci. U.S.A.* **117**, 22068–22079 (2020).
45. L. Wan *et al.*, MTDH-SND1 interaction is crucial for expansion and activity of tumor-initiating cells in diverse oncogene- and carcinogen-induced mammary tumors. *Cancer Cell* **26**, 92–105 (2014).
46. G. Hu *et al.*, MTDH activation by 8q22 genomic gain promotes chemoresistance and metastasis of poor-prognosis breast cancer. *Cancer Cell* **15**, 9–20 (2009).
47. R. M. L. Queiroz *et al.*, Comprehensive identification of RNA-protein interactions in any organism using orthogonal organic phase separation (OOPS). *Nat. Biotechnol.* **37**, 169–178 (2019).
48. X. Meng *et al.*, Genetic deficiency of mtdh gene in mice causes male infertility via impaired spermatogenesis and alterations in the expression of small non-coding RNAs. *J. Biol. Chem.* **290**, 11853–11864 (2015).
49. K. Valencia *et al.*, The Mir181ab1 cluster promotes KRAS-driven oncogenesis and progression in lung and pancreas. *J. Clin. Invest.* **130**, 1879–1895 (2020).
50. M. Knarr *et al.*, miR-181a initiates and perpetuates oncogenic transformation through the regulation of innate immune signaling. *Nat. Commun.* **11**, 3231 (2020).
51. Y. Lu *et al.*, Amplification and overexpression of Hsa-miR-30b, Hsa-miR-30d and KHDRBS3 at 8q24.22-q24.23 in medulloblastoma. *PLoS One* **4**, e6159 (2009).
52. Z. Y. Lin *et al.*, MicroRNA-30d promotes angiogenesis and tumor growth via MYPT1/c-JUN/VEGFA pathway and predicts aggressive outcome in prostate cancer. *Mol. Cancer* **16**, 48 (2017).
53. M. Han *et al.*, microRNA-30d mediated breast cancer invasion, migration, and EMT by targeting KLF11 and activating STAT3 pathway. *J. Cell. Biochem.* **119**, 8138–8145 (2018).
54. T. Uziel *et al.*, The miR-17∼92 cluster collaborates with the sonic hedgehog pathway in medulloblastoma. *Proc. Natl. Acad. Sci. U.S.A.* **106**, 2812–2817 (2009).
55. S. Sengupta *et al.*, MicroRNA 92b controls the G1/S checkpoint gene p57 in human embryonic stem cells. *Stem Cells* **27**, 1524–1528 (2009).
56. L. K. Zhuang *et al.*, MicroRNA-92b promotes hepatocellular carcinoma progression by targeting Smad7 and is mediated by long non-coding RNA XIST. *Cell Death Dis.* **7**, e2203 (2016).

57. M. Li *et al.*, Exosomal miR-92b-3p promotes chemoresistance of small cell lung cancer through the PTEN/AKT pathway. *Front. Cell Dev. Biol.* **9**, 661602 (2021).
58. N. Zhukova *et al.*, Subgroup-specific prognostic implications of TP53 mutation in medulloblastoma. *J. Clin. Oncol.* **31**, 2927–2935 (2013).
59. C. H. Chau, B. R. O'Keefe, W. D. Figg, The canSAR data hub for drug discovery. *Lancet Oncol.* **17**, 286 (2016).
60. M. Shri, H. Agrawal, P. Rani, D. Singh, S. K. Onteru, Hanging drop, a best three-dimensional (3D) culture method for primary buffalo and sheep hepatocytes. *Sci. Rep.* **7**, 1203 (2017).
61. C. H. Hsu *et al.*, TET1 suppresses cancer invasion by activating the tissue inhibitors of metalloproteinases. *Cell Rep.* **2**, 568–579 (2012).
62. J. L. Rinn *et al.*, Functional demarcation of active and silent chromatin domains in human HOX loci by noncoding RNAs. *Cell* **129**, 1311–1323 (2007).
63. M. I. Love, W. Huber, S. Anders, Moderated estimation of fold change and dispersion for RNA-seq data with DESeq2. *Genome Biol.* **15**, 550 (2014).
64. K. L. Peng, A. M. Schmitt, Gene expression of depletion of lncRNA Miat in mouse stem-like MB cells. NCBI: GEO. https://www.ncbi.nlm.nih.gov/geo/query/acc.cgi?acc=GSE205691. Deposited 29 July 2022.
65. K.L. Peng, A. M. Schmitt, Gene expression of depletion of lncRNA Miat in mouse stem-like MB cells. NCBI: GEO. https://www.ncbi.nlm.nih.gov/geo/query/acc.cgi?acc=GSE205695. Deposited 29 July 2022.